Supporting Information

Promoting Ambient Ammonia Electrosynthesis on Modulated $Cu^{\delta+}$ Catalysts by B-Doping

Limin Wu, [a,b] Libing Zhang, [a,b] Shoujie Liu,[c] Jiaqi Feng,[a] Liang Xu,[a] Xingxing Tan, [a,b] Xiaodong Ma, [a,b] and Xiaofu Sun* [a,b]

[a.]Beijing National Laboratory for Molecular Sciences, CAS Key Laboratory of Colloid and Interface and Thermodynamics, CAS Research/Education Center for Excellence in Molecular Sciences, Institute of Chemistry, Chinese Academy of Sciences, Beijing 100190, China

E-mail: sunxiaofu@iccas.ac.cn

[b.]School of Chemical Sciences, University of Chinese Academy of Sciences, Beijing 100049, China

[c.]Chemistry and Chemical Engineering of Guangdong Laboratory, Shantou 515063, China

Experimental Section

1. Materials. Potassium nitrate-^{15}N (purity ≥ 99%) was obtained from Sigma-Aldrich Chemical Co., Ltd. Sodium salicylate (99 %), Toray Carbon Paper (CP, TGP-H-60, 19×19 cm), Nafion D-521 dispersion (5 % w/w in water and 1-propanol, ≥ 0.92 meg/g exchange capacity) and Nafion N-117 membrane (0.180 mm thick, ≥ 0.90 meg/g exchange capacity) were provided by Alfa Aesar China Co., Sodium borohydride (≥ 96%), Copper Chloride Dihydrate (99%) and sodium hypochlorite solution (≥ 5.2%) were purchased from Sinopharm Chemical Reagent Co., Ltd., P. R. China. Potassium nitrate-14N (≥ 99%) and Sodium nitroprusside dihydrate (≥ 99%) were obtained from Acros. Potassium Sulphate was provided by J&K Scientific Ltd. Sodium hydroxide and copper (60-100 nm) were obtained from Beijing InnoChem Science & Technology Co., Ltd.

2. Experimental Procedures

2.1 Preparation of Cu(B) samples. A simple one-step method was applied to synthesize the catalysts. In the process, copper chloride ($CuCl_2{\cdot}2H_2O$) and sodium borohydride ($NaBH_4$) were used as the precursors. The amount of $CuCl_2{\cdot}2H_2O$ affected the doping content of boron (Cu(B)-1: 400mg, Cu(B)-2: 300mg, Cu(B)-3: 100mg). Firstly, $CuCl_2$ was mixed with 2 mL H_2O; Secondly, 2 mL of 5M $NaBH_4$ was quickly added into 2mL $CuCl_2$ solution in an ice bath. Thirdly, when there were no bubbles forming, the as-synthesized catalysts were washed with deionized water and ethanol and then dried under vacuum overnight. Commercial nano-copper (60-100nm) was applied as another control sample. The synthesis of Cu(H) was adopted a procedure similar to the above method, but $NaBH_4$ was replaced by the same amount of hydrazine hydrate as the reducing reagent.

2.2 Characterization. The scanning electron microscopy (SEM) images were taken with a JEOL SU8020 system. The transmission electron microscopy (TEM) images, high-resolution transmission electron microscopy (HRTEM) images and energy-dispersive X-ray spectroscopic (EDS) elemental distribution mapping were obtained with JEOL JEM-2100F transmission electron microscope. The X-ray diffraction (XRD)

was measured via the X-ray diffractometer (Model D/MAX2500, Rigaka) using a Cu-Kα source. X-ray photoelectron spectrum (XPS) was acquired by the Thermo Scientific ESCA Lab 250Xi using 500 μm X-ray spot and 200 W monochromatic Al Kα radiation possessing a basic pressure of about 3×10^{-10} mbar in the analysis chamber. The C 1s peak at 284.8 eV was used for energy referencing of all binding energies. The ultraviolet-visible (UV-vis) absorbance spectra were tested on Perkin Elmer Lambda 1050+ spectrophotometer. The ^{1}H-NMR measurement was performed on Bruker Avance III 400 HD spectrometer. The X-ray absorption spectroscopy (XAS) measurements were conducted on the 4B9A beamline of the Beijing Synchrotron Radiation Facility (BSRF). And the test results were processed by Athena and Artemis. X-ray emission spectroscopy (XES) was performed on the 4W1B beamline of BSRF. Raman spectroscopy was conducted on the HORIBA LabRAM HR Evolution Raman microscope.

2.3 Electrode preparation. 10 mg as-prepared catalyst was mixed with 1 ml ethanol and 20 μl Nafion dispersion solution. Then, the mixture was sonicated for 30 min to form a homogeneous ink. 18 μL of the ink was quantitatively pipetted with a pipette gun and dropped onto a 0.5×1 cm^2 surface of carbon paper.

2.4 Electrochemical measurements. The electrochemical measurements were conducted by a CHI 660E (Shanghai CH Instruments Co., China) electrochemical workstation in an H-type electrolytic cell separated by a Nafion 117 proton exchange membrane. The as-synthesized samples on carbon paper, saturated Ag/AgCl electrode (RHE) was placed in the cathode chamber as the working electrode and reference electrode, respectively. And platinum net, placed in the anode chamber, was used as the counter electrode. The surface area of the working electrode was controlled with 1 cm^2. 0.5 M K_2SO_4 solution (37 mL) was regarded as the electrolyte of distributed to the anode. Meanwhile, and 0.5 M K_2SO_4 solution containing 0.01 M KNO_3 was added into the cathode compartment for NO_3^--reduction.

2.5 Determination of ion concentration.

Determination of ammonia-N:

50 μL of solution containing NaOH (0.75 M) and NaClO (ρ_{Cl} > 5.2%), 500 μL of solution containing 0.32 M NaOH and 0.4 M $C_7H_6O_3Na$, and 50 μL of $C_5FeN_6Na_2O$ solution (1 wt%) were respectively added into 4 mL electrolyte removed from the electrochemical reaction vessel. After standing for 2 h, the UV-Vis absorption spectrum was measured and the concentration-absorbance curves were calibrated by the standard NH_4Cl solution with a series of concentrations.

Determination of nitrite-N:

A mixture of p-aminobenzenesulfonamide (1 g), N-(1-Naphthyl) ethylenediamine dihydrochloride (0.1 g), ultrapure water (50 mL) and phosphoric acid (2.94 mL, ρ=1.70 g/mL) was used as a color reagent. A certain amount of electrolyte was taken out from the electrolytic cell and diluted to 3 mL to detection range. Next, 1 mL color reagent was added into the aforementioned 3 mL solution and mixed uniformity. Then the UV–Vis absorbance at 540 nm was recorded after 20min at room temperature. The concentration-absorbance curve was calibrated using a series of standard potassium nitrite solutions.

2.6 Isotope labeling experiments. We carried out the experiment using the same set-up over Cu(B)-2 with the addition of ^{15}N isotope-labeled nitrate. After the electrocatalytic reaction, the pH of electrolyte the resultant was adjust to 2~3. Then, 0.1 mL of the solution was thoroughly mixed with 0.6 mL of DMSO-d_6 for ^1H NMR.

2.7 Calculation of the Faradaic efficiency (FE), yield rate and half-cell energy efficiency (EE).

For nitrate electroreduction, the Faradaic efficiency was calculated by the Eq.1:

$$\text{Faradaic efficiency} = (8F \times c_{NH3} \times V) / (M_{NH3} \times Q) \quad (1)$$

The yield rate was defined from the electric charge consumed for synthesizing ammonia and total charge passed through the electrode according to Eq. 2:

$$Yield_{NH3} = (c_{NH3} \times V) / (M_{NH3} \times t \times m) \quad (2)$$

The half-cell energy efficiency (EE) was defined as the ratio of fuel energy to applied electrical power, which was calculated with the following Eq. 3:

$$EE_{NH3} = (1.23 - E^0_{NH3})\ FE/(1.23-E) \quad (3)$$

where F is the Faradaic constant (96485 C mol^{-1}), c_{NH3} is the mass concentration of NH_3(aq), V is the volume of electrolyte in the cathode compartment (37mL), M_{NH3} is the molar mass of NH_3, Q is the total charge passing the electrode. t is the electrolysis time (3 h), m is the mass of catalyst (0.18 mg). E^0_{NH3} represents the equilibrium potential of nitrate electroreduction to ammonia, which is 0.69 V. 1.23 V is the equilibrium potential of water oxidation (i.e. assuming the overpotential of the water oxidation is zero). E is the applied potential vs. RHE after 80% iR correction.

2.8 Electrochemical active surface area (ECSA) evaluation. Cyclic voltammetry (CV) curves in electrochemical double-layer capacitance (C_{dl}) determination were measured in a potential window nearly without the Faradaic process at different scan rates of 20, 40, 60, 80 and 100 mV s^{-1}. The plot of current density at set potential against scan rate has a linear relationship and its slope is the C_{dl}. ECSA could be determined by double-layer capacitance (C_{dl}) which was proportional to ECSA.

2.9 Differential Electrochemical Mass Spectrometry (DEMS) measurements. The prepared Cu(B)-2 sample dropped on the carbon paper of 0.6×0.6 cm^2, Ag/AgCl and Pt wire were applied as the working electrode, the reference electrode and the counter electrode, respectively. Ar was continuously pumped into the electrolyte containing 0.5 M K_2SO_4 and 0.01 M KNO_3. A constant potential of -0.7 V vs. RHE was applied throughout the test. 10 cycles were conducted in the same conditions to avoid the accidental error during the whole measurements.

3. Theoretical method

The present first principle DFT calculations are performed by Vienna Ab initio Simulation Package (VASP)[1] with the projector augmented wave (PAW) method.[2] The exchange-functional is treated using the generalized gradient approximation (GGA) of Perdew-Burke-Ernzerhof (PBE)[3] functional. The energy cutoff for the plane wave basis expansion was set to 450 eV and the force on each atom less than 0.02 eV/Å was set for convergence criterion of geometry relaxation. A 15 Å vacuum was added along the z direction in order to avoid the interaction between periodic structures. The Brillouin zone integration is performed using 3×3×1 k-point sampling. The self-consistent

calculations apply a convergence energy threshold of 10^{-5} eV. The DFT-D3 method was employed to consider the van der Waals interaction.[4]

The free energies of the NO_3- reduction reaction steps (NO_3RR) were calculated by the equation: $\Delta G = \Delta E_{DFT} + \Delta E_{ZPE} - T\Delta S$, where ΔE_{DFT} is the DFT electronic energy difference of each step, ΔE_{ZPE} and ΔS are the correction of zero-point energy and the variation of entropy, respectively, which are obtained by vibration analysis, T is the temperature (T = 300 K). [5]

Supplemental Figures

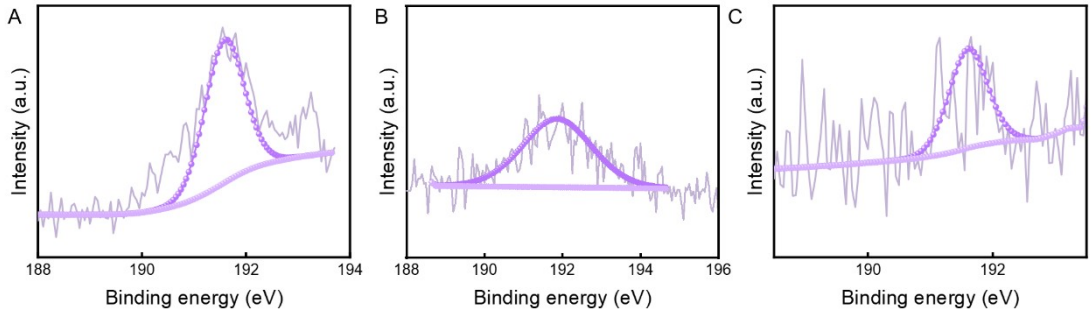

Figure S1. B electronic structure of (A) Cu(B)-1, (B) Cu(B)-2 and (C) Cu(B)-3 by XPS.

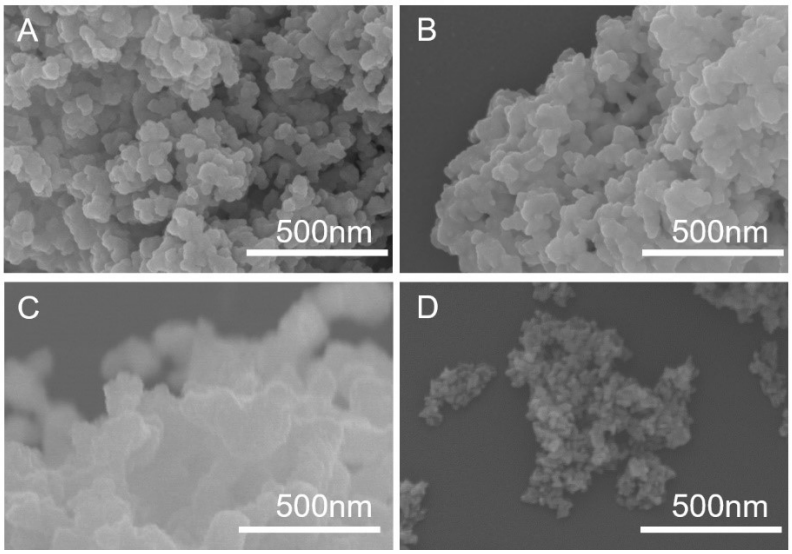

Figure S2. The SEM images for (A) Cu(B)-1, (B) Cu(B)-3, (C) Cu(C), and (D) Cu(H).

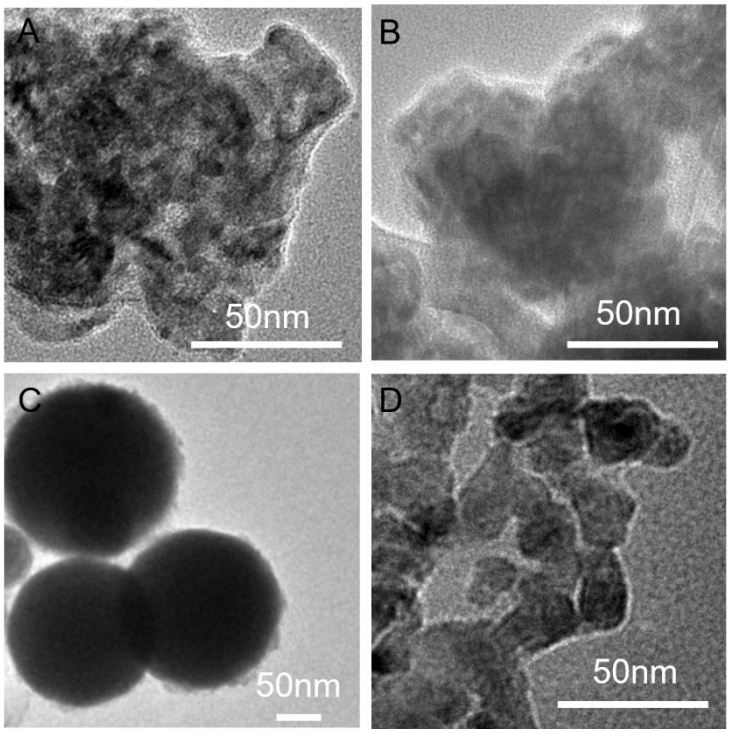

Figure S3. The TEM images for (A) Cu(B)-1, (B) Cu(B)-3, (C) Cu(C), and (D) Cu(H).

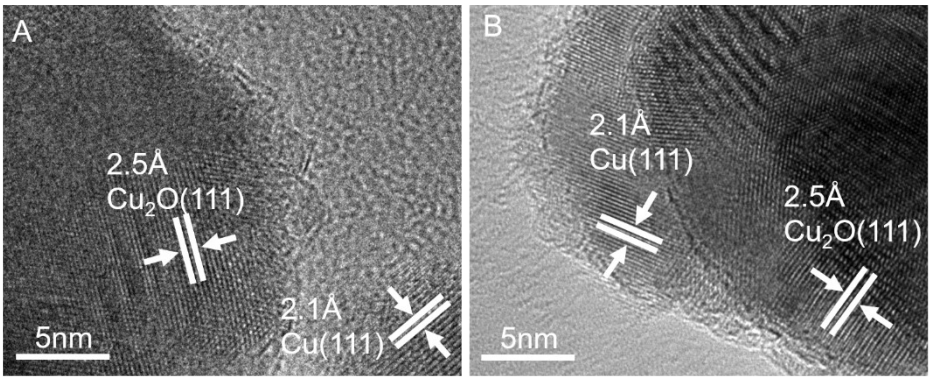

Figure S4. The HRTEM images for (A) Cu(B)-1and (B) Cu(B)-3.

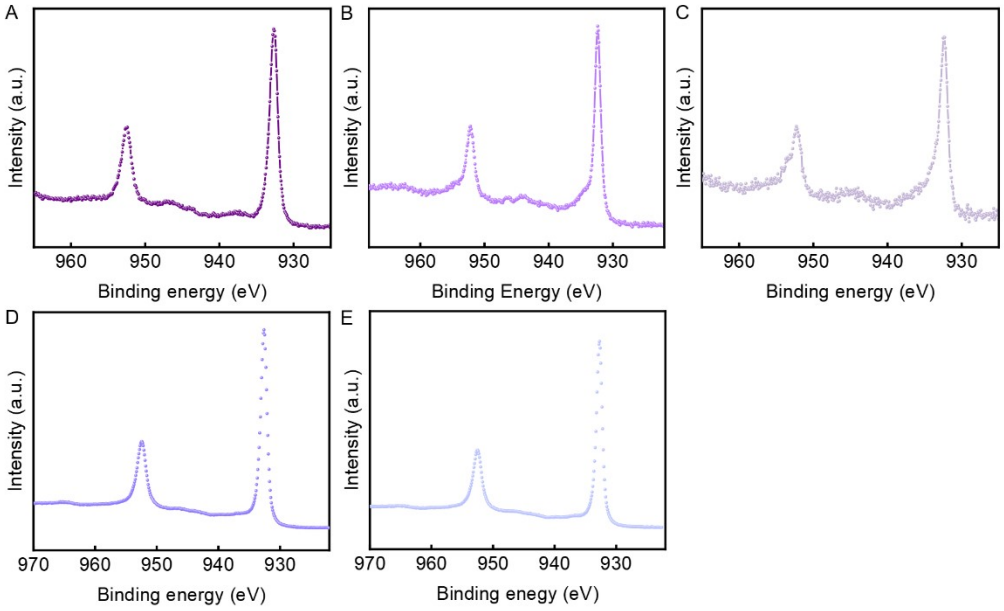

Figure S5. XPS Cu 2p spectra of (A) Cu(B)-1, (B) Cu(B)-2, (C) Cu(B)-3, (D) Cu(C), and (E) Cu(H).

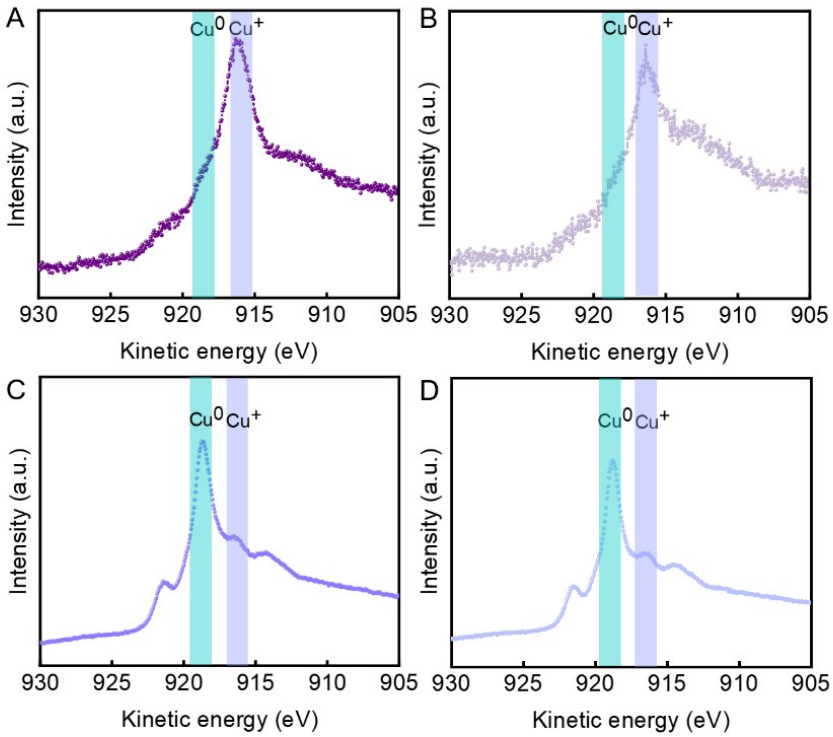

Figure S6. Cu LMM spectra of (A) Cu(B)-1, (B) Cu(B)-3, (C) Cu(C), and (D) Cu(H).

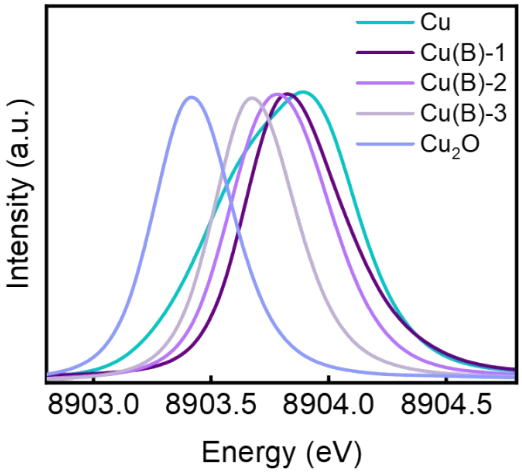

Figure S7. XES spectra of Cu(B)-1, Cu(B)-2 and Cu(B)-3.

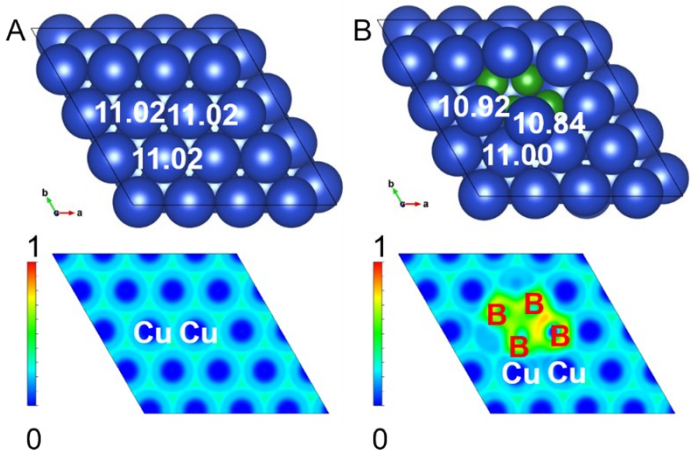

Figure S8. Bader charge analysis and election location function of (A) Cu(111) and (B) 4B-doped Cu(111).

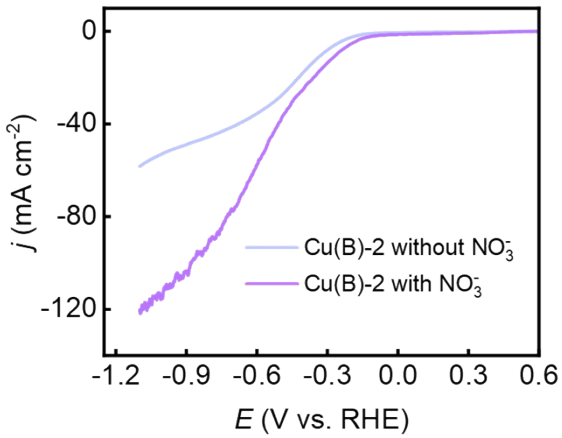

Figure S9. LSV curves of Cu(B)-2 during nitrate electroreduction in 0.5 M K_2SO_4 + 0.01 M ppm NO_3^-electrolyte with and without nitrate.

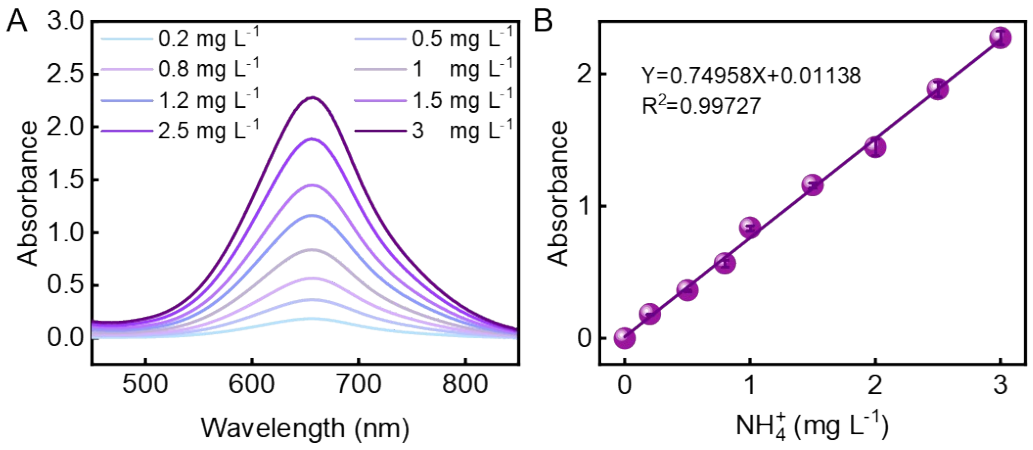

Figure S10. NH_3 quantification by UV−vis absorption spectroscopy. (A) UV−vis absorption spectra of various concentration of NH_4^+ using the indophenol blue method. (B) The corresponding standard calibration curve for the assessment of NH_3.

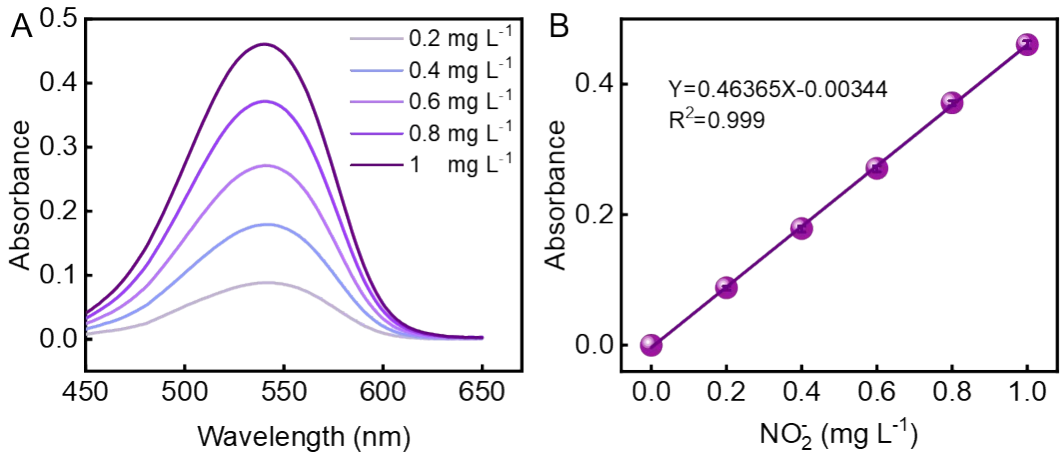

Figure S11. NO_2^- quantification by UV–vis absorption spectroscopy. (A) UV–vis absorption spectra of various concentration of NO_2^-. (B) The corresponding standard calibration curve for the assessment of NO_2^-.

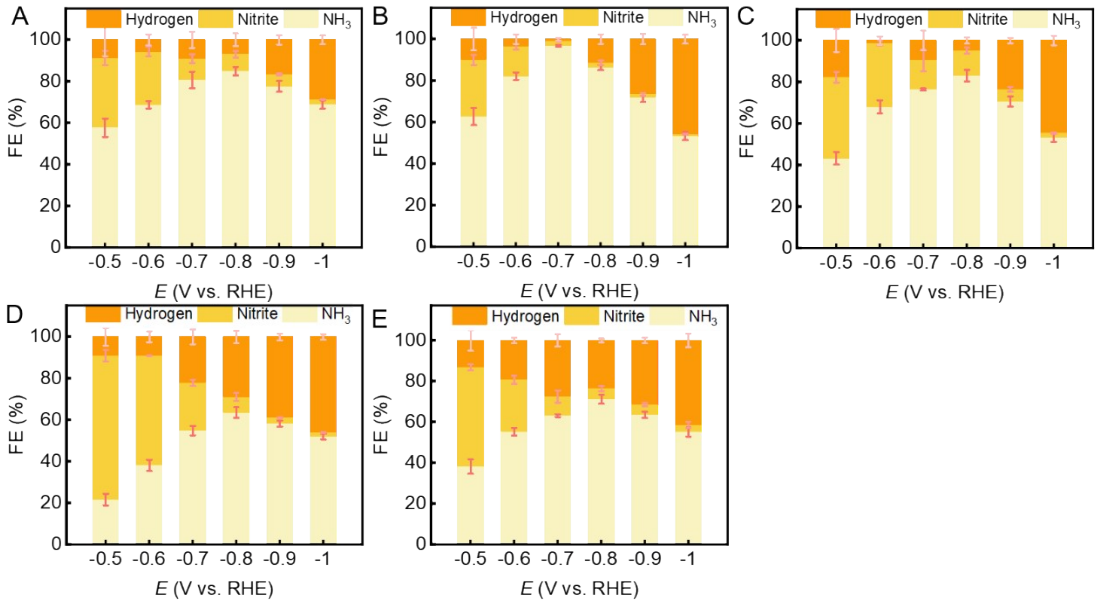

Figure S12. (A-E) FE of NH_3, NO_2^- and H_2 of Cu(B)-1, Cu(B)-2, Cu(B)-3, Cu(C) and Cu(H), respectively.

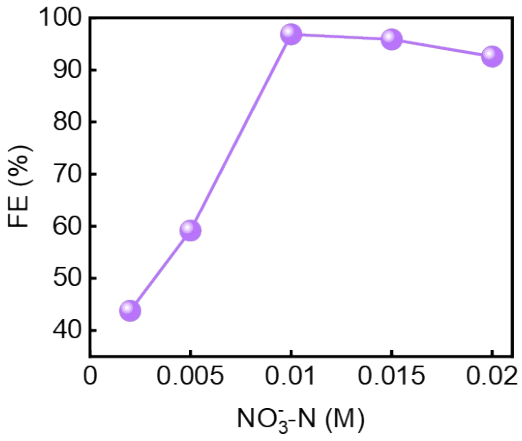

Figure S13. FE with various concentrations of nitrate.

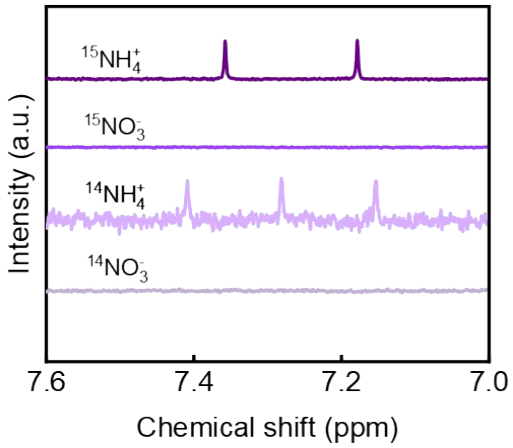

Figure S14. ^{1}H nuclear magnetic resonance (NMR) spectra of the electrolyte before and after electrocatalytic NO_3^--to-NH_3 over Cu(B)-2 at -0.7 V vs. RHE using $^{15}NO_3^-$ and $^{14}NO_3^-$ as the nitrogen source.

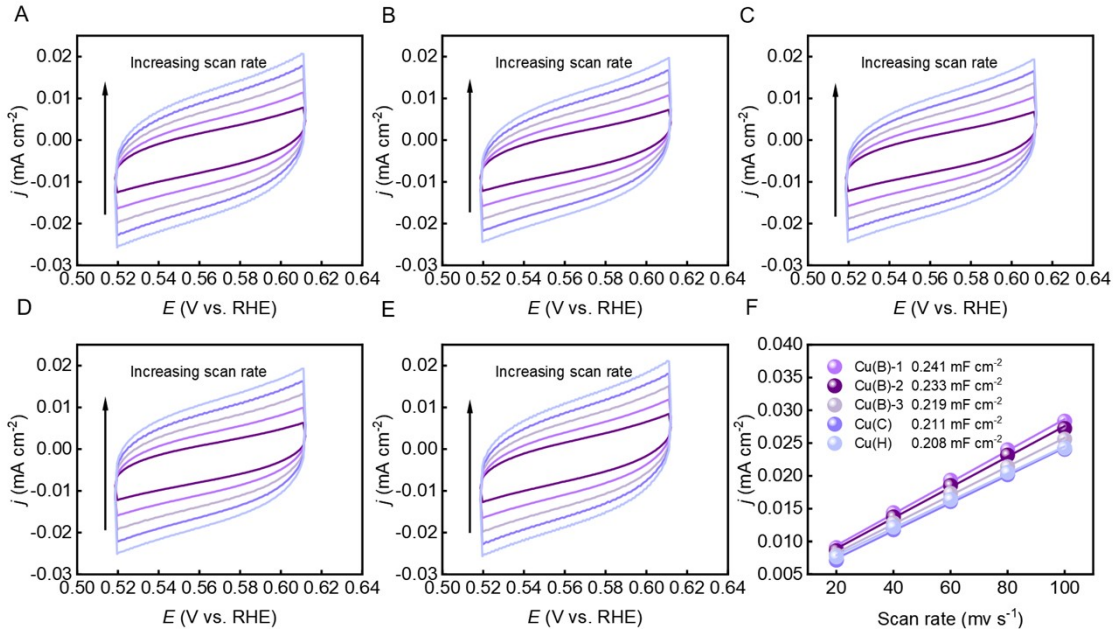

Figure S15. Cyclic voltammograms (CV) for (A) Cu(B)-1, (B) Cu(B)-2, (C) Cu(B)-3, (D) Cu(C) and (E) Cu(H) catalysts at different scan rates from 20 to 100 mV s^{-1}, respectively. (F) Plots showing the extraction of the C_{dl} for Cu(B)-1, Cu(B)-2, Cu(B)-3, Cu(C) and Cu(H), respectively.

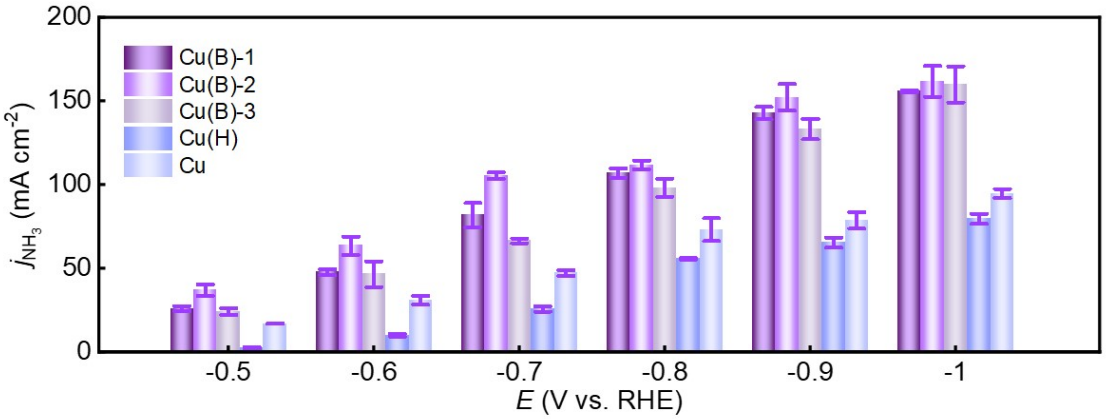

Figure S16. The current density from Figure 2C normalized to ECSA.

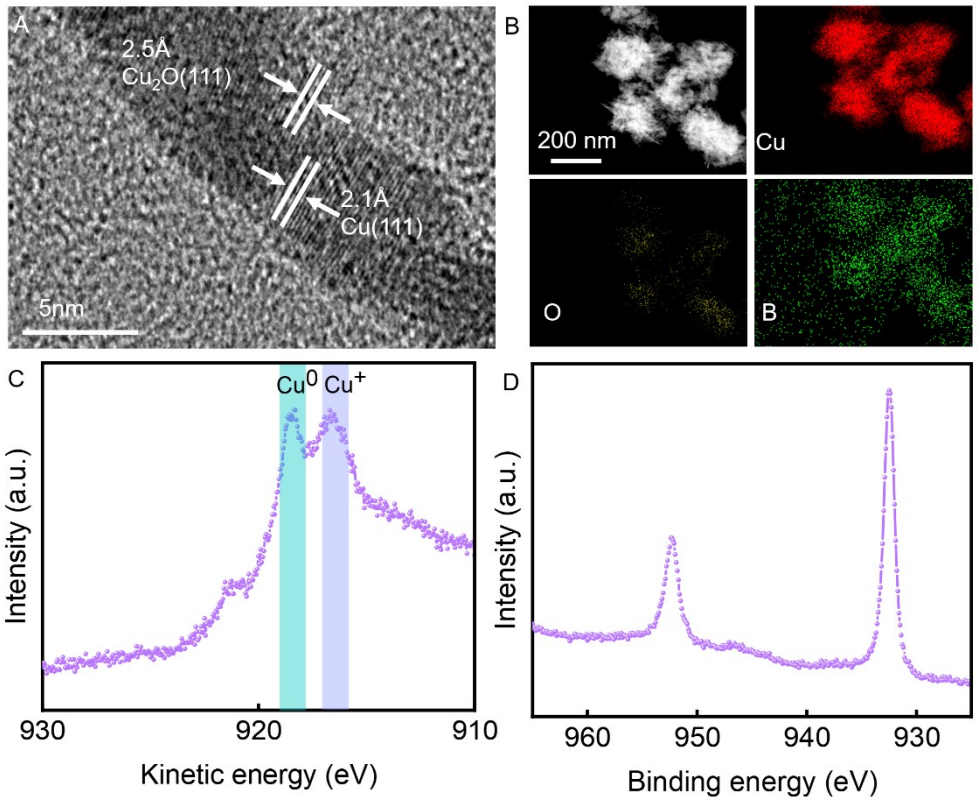

Figure S17. Characterization of Cu(B)-2 after electroreduction. (A) the HRTEM image; (B) EDS image; (C) Cu LMM spectra; (D) XPS Cu 2p spectra.

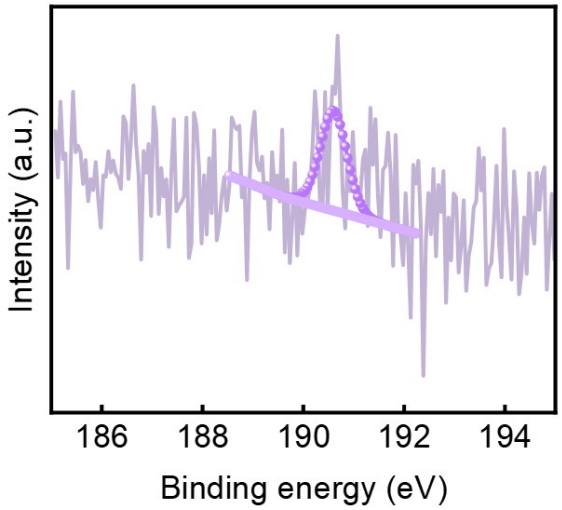

Figure S18. B electronic structure of Cu(B)-2 after electrosynthesis by XPS.

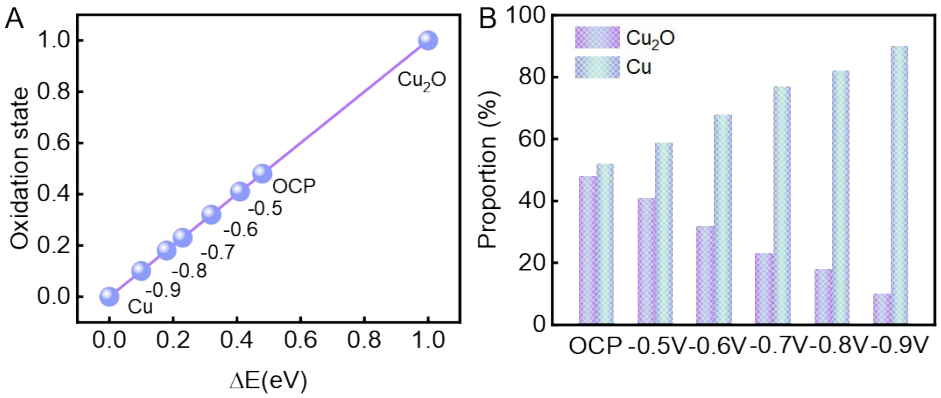

Figure S19. (A) Average oxidation state of copper in Cu(B)-2 after applying different potentials obtained from copper K-edge XANES. (B) Corresponding proportion of Cu and Cu_2O in Cu(B)-2 after applying different potentials.

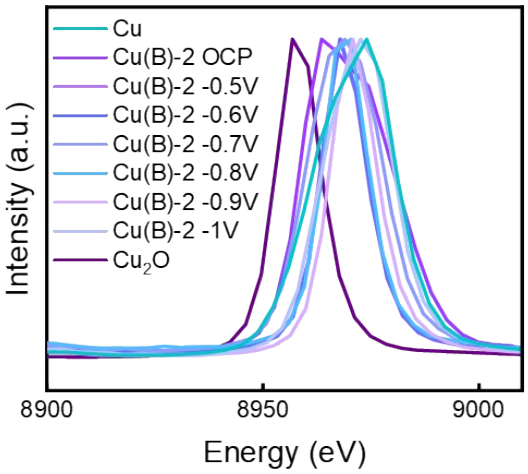

Figure S20. *In situ* XES spectra of Cu(B)-2 catalysts after applying different potentials.

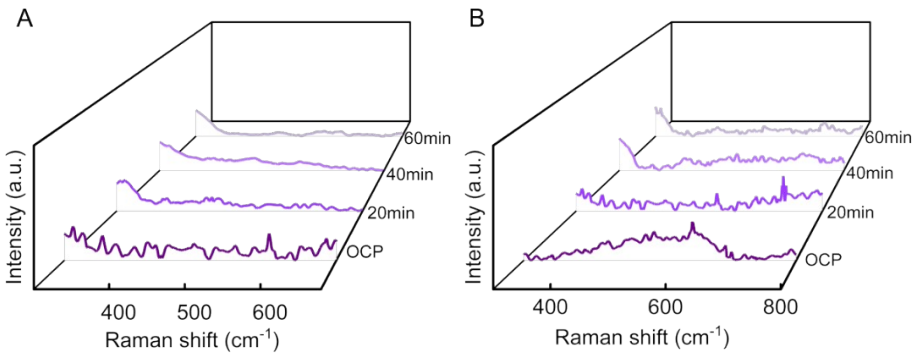

Figure S21. (A-B) *In situ* Raman spectra of Cu(C) and Cu(H) catalysts after 20 min, 40 min, and 60 min, respectively.

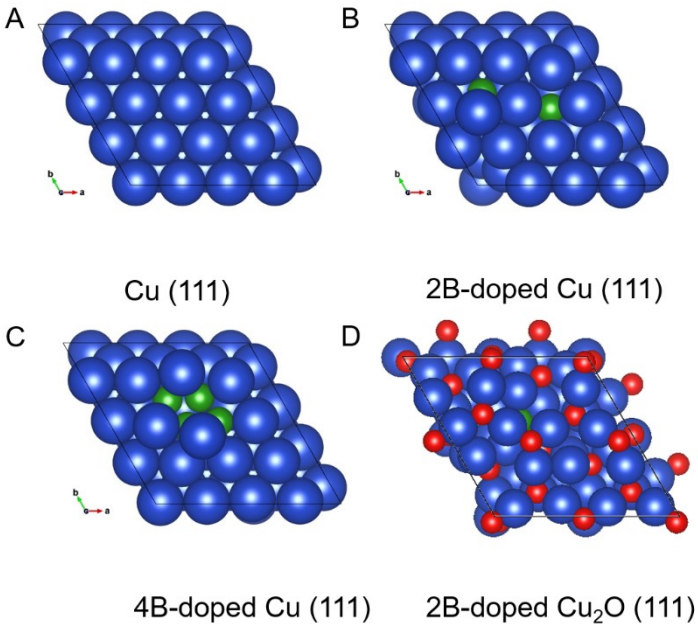

Figure S22. Stable structures of (A) Cu(111), (B) 2B-doped Cu(111), (C) 4B-doped Cu(111), and (D) 2B-doped-Cu_2O(111).

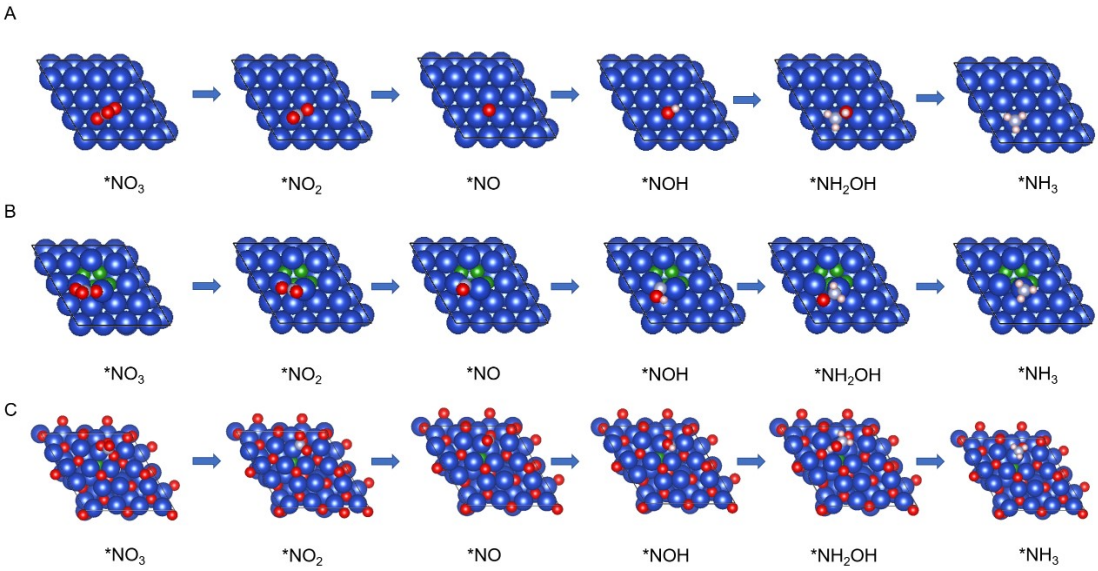

Figure S23. Stable configurations of the intermediates. The most stable adsorption configurations of *NO_3, *NO_2, *NO, *NOH, *NH_2OH, and *NH_3 on the surface of (A) Cu(111), (B) 4B-doped-Cu(111), and (C) 2B-doped-Cu_2O(111).

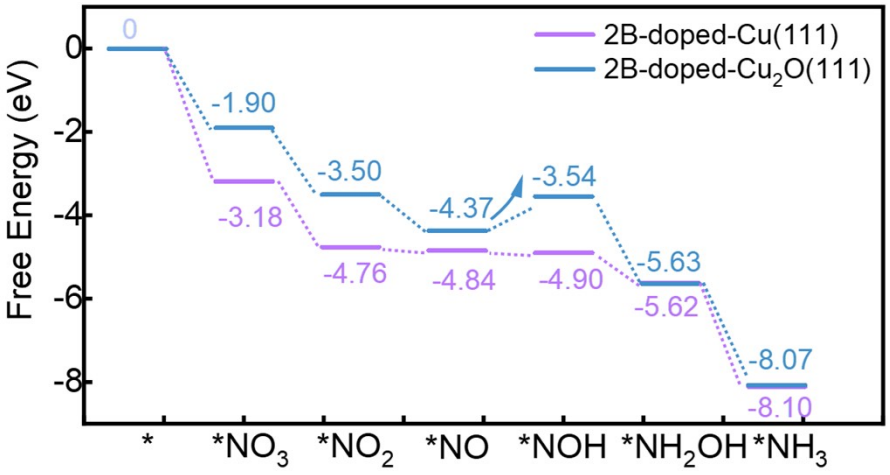

Figure S24. Gibbs free-energy diagrams of NO_3^--to-NH_3 over2B-doped-Cu(111) and 2B-doped-Cu_2O(111), respectively.

Table S1. Comparison of FE and yield rate by electrocatalytic nitrate reduction.

Catalysts	Electrolyte	Potential (V vs. RHE)	NH_3 yield rate	Faradaic Efficiency (%)	Ref.
Cu(B)-2	0.5 M K_2SO_4 and 1000 ppm NO_3^-	-0.7	7.2 mg h^{-1} $mg_{cat.}^{-1}$ (-0.7 V) 11.1 mg h^{-1} $mg_{cat.}^{-1}$ (-1 V)	96.8	This work
Cu/Cu_2O NWAs on Cu mesh	0.5 M Na_2SO_4 and 200 ppm NO_3^-	-0.85	0.2449 mmol h^{-1} cm^{-2}	81	[6]
HSCu-AGB@C	1 M KOH + 0.1 M NO_3^-	-0.2	487.8 mmol $g^{-1}_{cat.}$ h^{-1}	94.2	[7]
PTCDA/O–Cu on carbon cloth	0.1 M PBS and 500 ppm NO_3^-	-0.4	436 ± 85 μg h^{-1} cm^{-2}	77 ± 3	[8]
CuCoSP on Cu foil	0.1 M KOH and 0.01 M NO_3^-	-0.175	2642.9 ± 104.7 μg h^{-1} cm^{-2}	94.2 ± 1.7	[9]
CuNi alloy on Cu foam	1 M KOH and 0.1 M NO_3^-	-0.1	NH_3 partial current density 90 mA cm^{-2}	~95	[10]
Co/CoO NSAS on Ni foam	0.1 M Na_2SO_4 and 200 ppm NO_3^-	-1.3 V vs. SCE (~-0.64 V vs. RHE)	194.46 μmol h^{-1} cm^{-2}	~93.8	[11]
Strained Ru nanoclusters	1 M KOH and 1 M NO_3^-	-0.2	1.17 mmol h^{-1} cm^{-2}	~100	[12]
TiO_2 nanotubes with oxygen vacancies on Ti foil	0.5 M Na_2SO_4 and 50–200 ppm NO_3^-	-1.3 V vs. SCE (~-0.94 V vs. RHE)	0.045 mmol h^{-1} mg^{-1}	95.2	[13]
Ti foil	0.4 M NO_3^- at pH = ~0.77	-1.0	NH_3 partial current density 22 mA cm^{-2}	82	[14]
Fe single atom	0.50 M KNO_3 and 0.10 M K_2SO_4	-0.66 -0.85	5245 μg h^{-1} $mg_{cat.}^{-1}$ 20000 μg h^{-1} $mg_{cat.}^{-1}$	75	[15]
Cu-Pt bimetallic 3D-electrocatalyst	0.1 mol L^{-1} Na_2SO_4 and 10 mmol L^{-1} $NaNO_3$		194.4 $mg_{NH3\text{-}N}$ L^{-1} $g_{cat.}^{-1}$	94	[16]
Fe/Ni_2P	0.2 M K_2SO_4 and 50×10^{-3} M KNO_3	-0.4	4.17 mg_{NH3} h^{-1} cm^{-2}	94.3	[17]
***In situ* grown Fe_3O_4 particle**	0.1 M NaOH and 0.1 M $NaNO_3$	-0.5	10,145 μg h^{-1} cm^{-2}	91.5	[18]

$NiCo_2O_4$ nanowire array on carbon cloth	0.1 M $NaNO_3$ and 0.1 M NaOH		973.2 μmol h^{-1} cm^{-2} (-0.6 V)	99 (-0.3 V)	[19]
Co_3O_4@NiO HNTs	200 ppm NO_3^--N + 0.5 M Na_2SO_4		0.00693 mmol h^{-1} mg^{-1}	54.97	[20]
In-S-G	1 M KOH and 0.1 M KNO_3	-0.5	220 mmol h^{-1} g^{-1}	75	[21]
Cu@Cu_{2+1}O NWs/CP	0.5 M K_2SO_4 and 50 mg L^{-1} NO_3^-	-1.2 V vs. saturated calomel electrode	576.53 μg h^{-1} mg^{-1}	87.07	[22]
CuPd (3:1) aerogels	0.5 M K_2SO_4 and 50 mg L^{-1} NO_3^-	-0.46	784.37 μg h^{-1} mg^{-1}	90.02	[23]
Defect-rich Cu nanoplates	0.5 M K_2SO_4 and 50 ppm NO_3^-	-1.3 V vs. SCE (~-0.94 V vs. RHE)	781.25 μg h^{-1} mg^{-1}	85.47	[24]
Fluorine doped carbon	0.05 M H_2SO_4 and 200 ppm KNO_3	-0.65	23.8 mmol h^{-1} g^{-1}	20	[25]
NbO_x	0.5M Na_2SO_4 and 1000 ppm KNO_3	-0.75	55.0 μg h^{-1} mg^{-1}	94.5	[26]
Cu nanosheets	0.1 M KOH and 10 mM of KNO_3	-0.15	390.1 μg h^{-1} mg^{-1}	99.7	[27]

Table S2. Comparison of FE and yield rate by electrocatalytic nitrogen reduction.

Catalysts	Electrolyte	Potential (V vs. RHE)	NH_3 yield rate	Faradaic Efficiency (%)	Ref.
Ru single-atom catalysts	0.05 M H_2SO_4	-0.2	120.9 $\mu g\ h^{-1}\ mg^{-1}$	29.6	[28]
$FeMo_3S_4$ nanorods	0.5 M $LiClO_4$	-0.3	65.3 $\mu g\ h^{-1}\ mg^{-1}$	19.2	[29]
Donor–acceptor couples of Ni and Au nanoparticles	0.05 M H_2SO_4	-0.14	7.4 $\mu g\ h^{-1}\ mg^{-1}$	67.8	[30]
PdRu porous nanostructures	0.1 M HCl	-0.1	25.92 $\mu g\ h^{-1}\ mg^{-1}$	1.53	[31]
Single Mo atom anchored on N-doped carbon	0.05 M H_2SO_4	-0.45	69.2 $\mu g\ h^{-1}\ mg^{-1}$	24.8	[32]
CrN nanocube	0.1 M HCl	-0.5	31.11 $\mu g\ h^{-1}\ mg^{-1}$	16.6	[33]

Supplemental References

1. G. Kresse and J. Furthmüller, *Comput. Mater. Sci.*, 1996, **6**, 15-50.
2. P. E. Blöchl, *Phys. Rev. B*, 1994, **50**, 17953-17979.
3. J. P. Perdew, J. A. Chevary, S. H. Vosko, K. A. Jackson, M. R. Pederson, D. J. Singh and C. Fiolhais, *Phys. Rev. B*, 1992, **46**, 6671-6687.
4. S. Grimme, J. Antony, S. Ehrlich and H. Krieg, *J. Chem. Phys.*, 2010, **132**, 154104.
5. S. L. Dudarev, G. A. Botton, S. Y. Savrasov, C. J. Humphreys and A. P. Sutton, *Phys. Rev. B*, 1998, **57**, 1505-1509.
6. Y. Wang, W. Zhou, R. Jia, Y. Yu and B. Zhang, *Angew. Chem. Int. Ed.*, 2020, **59**, 5350-5354.
7. Q. Hu, Y. Qin, X. Wang, H. Zheng, K. Gao, H. Yang, P. Zhang, M. Shao and C. He, *CCS Chem.*, 2022, **4**, 2053-2064.
8. G.-F. Chen, Y. Yuan, H. Jiang, S.-Y. Ren, L.-X. Ding, L. Ma, T. Wu, J. Lu and H. Wang, *Nat. Energy*, 2020, **5**, 605-613.
9. W. He, J. Zhang, S. Dieckhofer, S. Varhade, A. C. Brix, A. Lielpetere, S. Seisel, J. R. C. Junqueira and W. Schuhmann, *Nat. Commun.*, 2022, **13**, 1129.
10. Y. Wang, A. Xu, Z. Wang, L. Huang, J. Li, F. Li, J. Wicks, M. Luo, D.-H. Nam, C.-S. Tan, Y. Ding, J. Wu, Y. Lum, C.-T. Dinh, D. Sinton, G. Zheng and E. H. Sargent, *J. Am. Chem. Soc.*, 2020, **142**, 5702-5708.
11. Y. Yu, C. Wang, Y. Yu, Y. Wang and B. Zhang, *Sci. China Chem.*, 2020, **63**, 1469-1476.
12. J. Li, G. Zhan, J. Yang, F. Quan, C. Mao, Y. Liu, B. Wang, F. Lei, L. Li, A. W. M. Chan, L. Xu, Y. Shi, Y. Du, W. Hao, P. K. Wong, J. Wang, S.-X. Dou, L. Zhang and J. C. Yu, *J. Am. Chem. Soc.*, 2020, **142**, 7036-7046.
13. R. Jia, Y. Wang, C. Wang, Y. Ling, Y. Yu and B. Zhang, *ACS Catal.*, 2020, **10**, 3533-3540.
14. J. M. McEnaney, S. J. Blair, A. C. Nielander, J. A. Schwalbe, D. M. Koshy, M. Cargnello and T. F. Jaramillo, *ACS Sustain. Chem. Eng.*, 2020, **8**, 2672-2681.
15. P. Li, Z. Jin, Z. Fang and G. Yu, *Energy Environ. Sci.*, 2021, **14**, 3522-3531.
16. G. A. Cerrón-Calle, A. S. Fajardo, C. M. Sánchez-Sánchez and S. Garcia-Segura, *Appl. Catal. B: Environ.*, 2022, **302**, 120844.
17. R. Zhang, Y. Guo, S. Zhang, D. Chen, Y. Zhao, Z. Huang, L. Ma, P. Li, Q. Yang, G. Liang and C. Zhi, *Adv. Energy Mater.*, 2022, **12**, 2103872.
18. X. Fan, L. Xie, J. Liang, Y. Ren, L. Zhang, L. Yue, T. Li, Y. Luo, N. Li, B. Tang, Y. Liu, S. Gao, A. A. Alshehri, Q. Liu, Q. Kong and X. Sun, *Nano Res.*, 2022, **15**, 3050-3055.
19. Q. Liu, L. Xie, J. Liang, Y. Ren, Y. Wang, L. Zhang, L. Yue, T. Li, Y. Luo, N. Li, B. Tang, Y. Liu, S. Gao, A. A. Alshehri, I. Shakir, P. O. Agboola, Q. Kong, Q. Wang, D. Ma and X. Sun, *Small*, 2022, e2106961.
20. Y. Wang, C. Liu, B. Zhang and Y. Yu, *Sci. China Mater.*, 2020, **63**, 2530-2538.
21. F. Lei, W. Xu, J. Yu, K. Li, J. Xie, P. Hao, G. Cui and B. Tang, *Chem. Eng. J.*, 2021, **426**, 131317.
22. T. Ren, K. Ren, M. Wang, M. Liu, Z. Wang, H. Wang, X. Li, L. Wang and Y. Xu, *Chem. Eng. J.*, 2021, **426**, 130759.
23. Y. Xu, K. Ren, T. Ren, M. Wang, M. Liu, Z. Wang, X. Li, L. Wang and H. Wang, *Chem. Commun.*, 2021, **57**, 7525-7528.
24. Y. Xu, M. Wang, K. Ren, T. Ren, M. Liu, Z. Wang, X. Li, L. Wang and H. Wang, *J. Mater. Chem. A*, 2021, **9**, 16411-16417.
25. Y. Li, S. Xiao, X. Li, C. Chang, M. Xie, J. Xu and Z. Yang, *Mater. Today Phys.*, 2021, **19**, 100431.
26. X. Wan, W. Guo, X. Dong, H. Wu, X. Sun, M. Chu, S. Han, J. Zhai, W. Xia, S. Jia, M. He and B. Han, *Green Chem.*, 2022, **24**, 1090-1095.
27. X. Fu, X. Zhao, X. Hu, K. He, Y. Yu, T. Li, Q. Tu, X. Qian, Q. Yue, M. R. Wasielewski and Y. Kang, *Appl. Mater. Today*, 2020, **19**, 100620.
28. Z. Geng, Y. Liu, X. Kong, P. Li, K. Li, Z. Liu, J. Du, M. Shu, R. Si and J. Zeng, *Adv Mater*, 2018, e1803498.

29. J. Wang, H. Nan, Y. Tian and K. Chu, *ACS Sustain. Chem. Eng.*, 2020, **8**, 12733-12740.
30. Z.-H. Xue, S.-N. Zhang, Y.-X. Lin, H. Su, G.-Y. Zhai, J.-T. Han, Q.-Y. Yu, X.-H. Li, M. Antonietti and J.-S. Chen, *J. Am. Chem. Soc.*, 2019, **141**, 14976-14980.
31. Z. Wang, C. Li, K. Deng, Y. Xu, H. Xue, X. Li, L. Wang and H. Wang, *ACS Sustain. Chem. Eng.*, 2018, **7**, 2400-2405.
32. C. Ling, X. Bai, Y. Ouyang, A. Du and J. Wang, *J. Phys. Chem. C*, 2018, **122**, 16842-16847.
33. Z. Ma, J. Chen, D. Luo, T. Thersleff, R. Dronskowski and A. Slabon, *Nanoscale*, 2020, **12**, 19276-19283.